analysing the size of the charge pulse produced, the energy of the photon is determined. The powder-diffraction pattern is recorded as a function of energy (typically somewhere within the range 10–150 keV, depending on the source) *via* a multichannel analyser (MCA). Instruments may have multiple detectors, at different 2θ angles covering different ranges in d-spacing (Barnes *et al.*, 1998), or arranged around a Debye–Scherrer ring, as in the 23-element semi-annular detector at beamline I12 at Diamond Light Source (Korsunsky *et al.*, 2010; Rowles *et al.*, 2012).

Prior to performing the EDD experiment, the detector and MCA system must be calibrated, *e.g.* by measuring signals from sources of known energy, such as ^{241}Am (59.5412 keV) or ^{57}Co (122.06014 and 136.4743 keV) at hard energies, and/or from the fluorescence lines of elements such as Mo, Ag, Ba *etc*. The 2θ angle also needs to be calibrated if accurate d-spacings are desired. This should be done by measuring the diffraction pattern of a standard sample with known d values.

The detector angle is typically chosen in the range 2–6° 2θ and influences the range of d-spacings accessible *via* the term $1/\sin\theta$, *i.e.* the lower the angle, the higher the energy needed to access any particular d. Normally, the range of most interest should be matched to the incident spectrum, taking account also of sample absorption and fluorescence, to produce peaks with high intensity. More than one detector at different angles can also be employed. Energy-sensitive Ge detectors do not count particularly fast, up to 50 kHz being a typical value compared to possibly 1–2 MHz with a scintillation detector. Hence they are relatively sensitive to pulse pile-up and other effects of high count rates (Cousins, 1994; Laundy & Collins, 2003; Honkimäki & Suortti, 2007), particularly if the synchrotron is operating in a mode with a few large electron bunches giving very intense pulses of X-rays on the sample.

The energy resolution of the detector is of the order of 2%, which dominates the overall resolution of the technique. Its main uses are where a fixed geometry with penetrating X-rays is required, *e.g.* in high-pressure cells, for *in situ* studies (Häusermann & Barnes, 1992), *e.g.* of chemical reactions under hydrothermal conditions (Walton & O'Hare, 2000; Evans *et al.*, 1995), electrochemistry (*e.g.* Scarlett *et al.*, 2009; Rijssenbeek *et al.*, 2011; Rowles *et al.*, 2012), or measurements of residual strain (Korsunsky *et al.*, 2010). Owing to the use of polychromatic radiation, the technique has very high flux on the sample and can be used for high-speed data collection, following rapid processes *in situ*. However, accurate modelling of the intensities of the powder-diffraction pattern for structural or phase analysis is difficult because of the need to take several energy-dependent effects into account, *e.g.* absorption and scattering factors, the incident X-ray spectrum, and the detector response. Nevertheless, examples where this has been successfully carried out have been published (*e.g.* Yamanaka & Ogata, 1991; Scarlett *et al.*, 2009).

A higher-resolution variant of the energy-dispersive technique can be performed by using a standard detector behind a collimator at fixed 2θ scanning the incident energy *via* the monochromator. The Hart–Parrish design with long parallel foils is suitable. Such an approach has been demonstrated in principle (Parrish, 1988), but is rarely used in practice. The advantage is to be able to measure data of improved d-spacing resolution, as compared to using an energy-dispersive detector, from sample environments with highly restricted access. In principle, as a further variant, white incident radiation could be used with scanning of θ_a, the angle of the analyser crystal, and associated detector at $2\theta_a$, all at fixed 2θ.

2.2.5. Considerations for powder-diffraction experiments

Synchrotron radiation allows considerable flexibility for a powder-diffraction experiment, offering choice and optimization of a number of quantities such as the wavelength, with high energy resolution, range in d-spacing, angular resolution, angular accuracy, and spatial or time resolution (but not all of these can necessarily be optimized at the same time). Increasingly, powder-diffraction experiments at synchrotrons are combined with complementary measurements, simultaneously applying techniques such as Raman spectroscopy (Boccaleri *et al.*, 2007; Newton & van Beek, 2010), particularly when carrying out *in situ* studies of an evolving system. In this respect, the open nature of a synchrotron instrument, with space around the sample to position auxiliary equipment, is an advantage.

2.2.5.1. *Polarization*

Assuming the beam is 100% polarized in the horizontal plane of the synchrotron orbit and with detection in the vertical plane, there is no need for any polarization correction to the diffracted intensities. However, if a small amount of vertical polarization of the beam does need to be taken into account (possibly up to a few per cent depending on the source), the polarization factor that describes its effect on the intensity of the diffracted beam can be derived, following the approach of Azároff (1955) and Yao & Jinno (1982), as

$$P = \frac{1 - dp + dp\cos^2 2\theta\cos^2 2\theta_a}{1 - dp + dp\cos^2 2\theta_a} = \frac{1 - dp + dp\cos^2 2\theta\cos^2 2\theta_a}{1 - dp\sin^2 2\theta_a}, \tag{2.2.3}$$

where dp is the depolarization fraction (*i.e.* the fraction of the total intensity incident on the sample that is vertically polarized), $2\theta_a$ is the Bragg angle of the analyser crystal (if any), and the denominator scales P to unity at 2θ equal to zero (Dwiggins, 1983) and is a constant for any particular experimental setup. If there is no analyser crystal, or we ignore the effect it would have (*i.e.* by putting $2\theta_a = 0$), then

$$P = 1 - dp\sin^2 2\theta.$$

Beamline staff can usually advise on the appropriate values to use. These expressions reduce to the usual polarization factor for unpolarized (dp = 0.5) laboratory X-rays without a monochromator or analyser crystal, $\frac{1}{2}(1 + \cos^2 2\theta)$.

An alternative formulation of equation (2.2.3) considers the ratio of the vertical to horizontal polarization,

$$rp = \frac{dp}{1 - dp} \quad \text{and} \quad dp = \frac{rp}{1 + rp},$$

so that

$$P = \frac{1 + rp\cos^2 2\theta\cos^2 2\theta_a}{1 + rp\cos^2\theta_a}. \tag{2.2.4}$$

Note that rp = 1.0 for unpolarized (laboratory) X-rays. In reality, because the synchrotron beam is near 100% plane polarized, dp and rp have similar values. The same expressions can be used if diffracting and analysing in the horizontal plane, except that now the value of dp or rp is replaced with the value of $(1 - dp)$ or $1/rp$, respectively.

For Debye–Scherrer rings detected on a 2D detector, the azimuthal angle around the ring needs to be taken into account, yielding

$$P = (1 - dp)(\cos^2 2\theta \sin^2 \kappa + \cos^2 \kappa) + dp(\cos^2 2\theta \cos^2 \kappa + \sin^2 \kappa)$$

or

$$P = \frac{(\cos^2 2\theta \sin^2 \kappa + \cos^2 \kappa) + rp(\cos^2 2\theta \cos^2 \kappa + \sin^2 \kappa)}{1 + rp},$$

where κ is the azimuthal angle (zero in the vertical direction) (Rowles *et al.*, 2012).

2.2.5.2. *Radiation damage*

The intensity of the incident beam can be so high that radiation damage becomes a real concern, particularly for samples containing organic molecules, such as pharmaceuticals, or organometallic materials. Radiation damage manifests itself by progressive shifts (often anisotropic) in the peak positions, a general reduction in peak intensities and peak broadening as the sample's crystallinity degrades. With high-resolution data, the effects are easily seen and can appear after only a few seconds in the worst cases. In such circumstances it may be better to use a 1D or 2D PSD to collect data of sufficient statistical quality before the damage is too severe. However, if the highest-resolution data are required, *via* scanning an analyser crystal, then the problem can be alleviated by filling a long capillary with sample and translating it between scans to expose fresh sample to the beam, thus acquiring multiple data sets which can be summed together. Such an approach necessarily requires a sufficient amount of disposable sample. If attempting to study the evolution of a particular part of the sample, *e.g.* undergoing heat treatment in the beam, then substituting fresh sample is not necessarily an option, and radiation damage can be a frustrating hindrance.

2.2.5.3. *Beam heating*

With a photon intensity of the order 10^{12} photons $\text{mm}^{-2}\,\text{s}^{-1}$ incident on the sample – a possible value for the unfocused beam on a beamline based on an insertion device at a modern third-generation source – the power in the beam corresponds to a few mW mm^{-2}. If a small fraction is absorbed by the sample this can represent a significant heat load that becomes troublesome when trying to work with samples at cryogenic temperatures, where heat capacities are relatively low.

As an example, consider a sample of microcrystalline silicon, composed of cubic 1 μm^3 grains irradiated by a 31 keV beam (0.4 Å wavelength) with 10^{12} photons $\text{mm}^{-2}\,\text{s}^{-1}$. The power of the beam is 5 mW mm^{-2} ($31 \times 10^3\ e \times 10^{12}$ W mm^{-2}). The mass absorption coefficient of Si at 0.4 Å wavelength $\mu/\rho \simeq 1.32\ \text{cm}^2\ \text{g}^{-1}$ (Milledge, 1968) leading to a linear absorption coefficient of $3.1\ \text{cm}^{-1}$ (density of Si = $2.33\ \text{g cm}^{-3}$). Any problems with absorption by such a sample might usually be discounted; for a 1-mm-diameter capillary the value of μr is 0.1, assuming the powder density is 2/3 of the theoretical density.

A single 1-μm^3 grain of cross section 1 μm^2 is hit by 10^6 photons s^{-1}, of which a small fraction are absorbed,

$$\begin{aligned}\text{photons absorbed} &= 10^6[1 - \exp(-3.1 \times 10^{-4})] \\ &= 310\ \text{photons s}^{-1},\end{aligned}$$

corresponding to an absorbed power of 1.54×10^{-12} W. Not all this energy is retained; significant amounts are lost as fluorescence, Compton scatter *etc*. Consultation of tables of mass attenuation coefficients and mass energy-absorption coefficients (Hubbell, 1982; Seltzer, 1993) indicates that for Si at 31 keV about 80% of the energy is retained, thus a net heating power of 1.2×10^{-12} W. The mass of the Si grain is 2.33×10^{-15} kg. At ambient temperature, where the specific heat capacity of Si is $704.6\ \text{J kg}^{-1}\,\text{K}^{-1}$, this leads to an instantaneous tendency to increase the temperature by $\sim 0.7\ \text{K s}^{-1}$. At cryogenic temperatures, *e.g.* 10 K, the specific heat capacity is over three orders of magnitude lower, $0.28\ \text{J kg}^{-1}\,\text{K}^{-1}$ (Desai, 1986), leading to a very strong tendency for the temperature to rise ($1840\ \text{K s}^{-1}$). The extent of the potential problem varies depending on the real net absorption of energy of the sample at the wavelength being used. However, it is clear that to prevent local beam-heating effects, the absorbed energy must be removed from the sample as efficiently as possible, *i.e.* by having excellent thermal contact between the grains of the sample and the external medium. At cryogenic temperatures this can be accomplished *via* the He exchange gas in the cryostat. Thus, if using a capillary sample, the capillary must either be left unsealed, to allow the He to permeate between the grains of sample, or it must be sealed under He, allowing transport of the heat to the walls of the capillary. Sealing under air, nitrogen, argon or other atmosphere leads to a loss of heat-transport capability when the gas solidifies, with consequent unpredictable behaviour for the sample caused by the beam-heating effects. This can involve significant shifts in peak positions and peak broadening depending on the instantaneous local temperature gradients. The problems tend to be worse at softer energies, where X-ray absorption is generally higher. Notwithstanding the potential problems, good-quality low-temperature data can be measured with appropriate care.

2.2.5.4. *Choice of wavelength*

The tunability of synchrotron radiation allows the wavelength best suited to the measurements to be selected. The collimation of the beam from the source combined with a perfect crystal monochromator lead automatically to high energy resolution, with a narrow wavelength distribution about a mean value. Consequently there are no issues to contend with such as α_1, α_2 doublets or other effects due to a composite incident spectrum, contributing to a relatively simple instrumental peak-shape function. High energy resolution is essential for high 2θ resolution, because, as shown in equation (2.2.1), the effect of the energy envelope is to broaden the diffraction peaks as 2θ increases.

In choosing the wavelength for an experiment, factors to consider include:

(*a*) The optimum operational range for the beamline to be used, which will principally depend on the characteristics of the source.

(*b*) Absorption: choosing a sufficiently hard energy generally reduces absorption and allows the use of a capillary specimen in transmission for a wide range of compounds, *e.g.* those containing transition metals or heavier elements, thus minimizing preferred orientation. Selecting the energy a little way below (in energy) the *K* or L_{III} absorption edge of an element in the sample may help minimize sample absorption. For any sample or series of samples, it is good practice in the planning of the experiment to calculate the linear absorption coefficient to assess the optimum capillary diameter, the wavelength to use and those to avoid.

(*c*) The use of hard energies can be advantageous for penetration through sample environments, although these should normally, as much as possible, be designed with appropriate X-ray windows *etc*. However, when absorbing environments are unavoidable, such as containing a sample in a spinning Pt

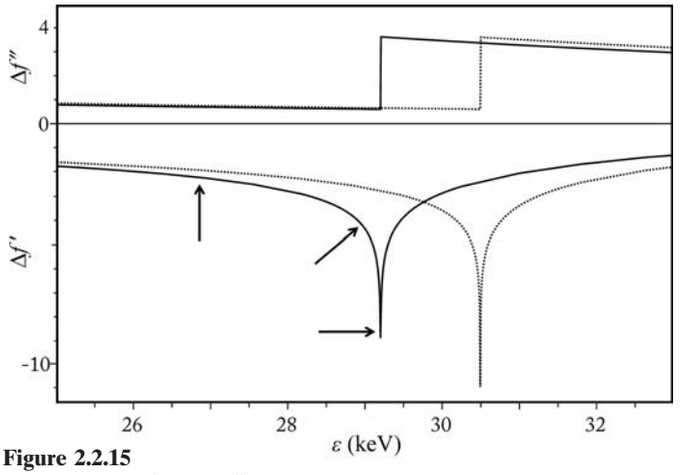

Figure 2.2.15
Variation of $\Delta f'$ and $\Delta f''$ with photon energy for Sn (solid line) and Sb (dotted line) in the vicinity of their *K* absorption edges (from the tables of Sasaki, 1989). An anomalous-scattering experiment seeking to distinguish the arrangement of the two elements could make measurements at the Sn edge (29.2001 keV), at a few eV below the edge and at an energy significantly removed from the edge (arrows). Equivalent measurements could be made at the Sb edge (30.4912 keV), but as this is above the energy of the Sn edge careful attention must be paid to the increase in the sample's absorption (reflected in the values of $\Delta f''$).

capillary for heating to very high temperatures, then high energy can be a major benefit.

(*d*) Hard energies are essential to measure to high Q values, where $Q = 4\pi \sin\theta/\lambda = 2\pi/d$. For pair distribution function (PDF) analysis, data to $Q > 25$ Å^{-1} ($d < 0.25$ Å) or more are required, with patterns of good statistical quality. Such Q values are not possible with Mo or Ag radiation (Ag $K\alpha$, λ = 0.56 Å, $Q \simeq 22$ Å^{-1} at $2\theta = 160°$), but are easily accessible at λ = 0.4 Å (31 keV) by scanning to $2\theta = 106°$. At 80.7 keV (0.154 Å, ten times shorter than Cu $K\alpha$) patterns to $Q \simeq 35$ Å^{-1} can be obtained in minutes (even seconds) with a large stationary medical-imaging flat-panel detector (Lee, Aydiner *et al.*, 2008). Even for more classical powder-diffraction experiments, access to data for high Q values can be advantageous for Rietveld refinement of crystal structures, or for measuring several orders of reflections for peak-shape analysis in the investigation of microstructure.

(*e*) Anomalous scattering: performing measurements near the absorption edge of an element in a sample and away from that edge gives element-specific changes in the diffraction intensities, enhancing the experiment's sensitivity to that element (Fig. 2.2.15). The approach can be complimentary to isotopic substitution in a neutron-diffraction experiment or may be the only option when no suitable isotope is available. Good energy resolution is important for these experiments. The values of $\Delta f'$ and $\Delta f''$ vary sharply over only a few eV at the edge, so poor energy resolution would average the abruptly changing values over too broad a range to the detriment of elemental sensitivity and sample absorption if part of the wavelength envelope strays above the edge. Moreover, it is necessary to know accurately where on the edge the measurement is being made to allow the correct values of $\Delta f'$ and $\Delta f''$ to be used in the data analysis. Tables of values have been calculated (*e.g.* Sasaki, 1989), but these do not take account of shifts in an edge due to the oxidation state(s) and chemical environment(s) of the elements. It is advisable to measure the fluorescence of the sample as the energy is scanned through the edge (by varying the monochromator angle θ_m) and then use the Kramers–Kronig relation to calculate the variation of $\Delta f'$ and $\Delta f''$ with energy. A program such as *CHOOCH* (Evans & Pettifer, 2001) allows this to be done.

(*f*) A wavelength greater than 1 Å may be best when working with large unit cells, such as found for proteins, organic molecules or organometallic compounds. Using a long wavelength helps by moving the diffraction pattern to higher 2θ values, away from the zone most affected by background air scatter or masked by the beam stop, and to where the peak asymmetry due to axial beam divergence is less severe. Longer wavelengths are also useful when working in reflection with plate samples to minimize beam penetration and thus enhance sensitivity to the surface regions, *e.g.* in the study of surfaces or coatings.

(*g*) The broad continuous spectrum available from a bending magnet or wiggler allows powder-diffraction measurements *via* the energy-dispersive approach, which is exploited when geometric considerations of the sample or environment mean that a restricted range of 2θ values is accessible or when attempting to obtain the maximum time resolution from a source, as a larger fraction of the photons from the source can be exploited.

2.2.5.5. *Angular resolution*

The highest angular resolution is obtained from a diffractometer equipped with an analyser crystal such as Si(111) or Ge(111). This also gives the robust parallel-beam optical configuration so that peak positions are accurately determined. For well crystallized high-quality samples, peak FWHMs of a few millidegrees are possible, thus maximizing the resolution of reflections with similar *d*-spacings. For less ideal samples, which represent the majority, microstructural effects broaden the peaks, and indeed high-resolution synchrotron data are exploited for detailed investigation of peak shapes and characterization of a range of properties such as crystallite size, microstrain (Chapter 5.2), defects, chemical homogeneity *etc*. Accurate high-resolution data are particularly useful for solving crystal structures from powders (Chapter 4.1), increasing the possibilities for indexing the powder diffraction pattern (Chapter 3.4), assessing the choice of possible space groups, and providing high-quality data for the structural solution and refinement steps. With a high-resolution pattern, the maximum amount of information is stored in the complex profile composed from the overlapping peaks.

2.2.5.6. *Spatial resolution*

Focusing the X-ray beam gives improved spatial resolution, *e.g.* for studying a small sample contained in a diamond anvil cell at high pressure. A beam with dimensions of a few μm can be obtained, though at the expense of the divergence of the beam arriving at the sample. In such cases the use of a 2D detector to record the entire Debye–Scherrer rings will be required to accumulate the diffraction pattern in a reasonable time and to reveal any problems with preferred orientation or granularity in the sample. With a very small sample only a few grains may be correctly oriented to provide each powder reflection. Alternatively, provided the intensity of the beam is high enough, simply cutting down the beam size with slits may be appropriate, *e.g.* to map residual strain in a weld or mechanical component where a spatial resolution on the 50–100 μm scale may be required. Smaller beam sizes may not be useful if they are comparable to the intrinsic grain size of the material, thus leading

to a poor statistical average of grain orientations and a spotty diffraction pattern.

2.2.5.7. *Time resolution*

The high flux allows powder-diffraction patterns to be measured quickly, opening up the possibilities for time-resolved studies, following the evolution of samples on a timescale, if appropriate, down to milliseconds, *e.g.* to investigate the kinetics and the mechanism of a phase transition caused by a change of the temperature, pressure or other external condition, or a chemical reaction taking place in the sample, such as self-propagating combustion synthesis (Labiche *et al.*, 2007). Many instruments allow great flexibility in the design of experiments to study systems *in situ*, helped by the availability of hard radiation to penetrate through sample environments and reduce the angular range that must be accessed to measure enough diffraction peaks to yield the desired information.

2.2.5.7.1. *Using fast detectors*

Scanning a detector through the d-spacing range of interest necessarily takes a few seconds, so is too slow to measure the fastest processes. Thus, for speed, a multichannel detector system is required that acquires the full diffraction pattern synchronously and that can be read out rapidly, such as *via* a fast PSD or using the energy-dispersive approach. Many different types of detector systems have been exploited for fast powder-diffraction studies using the monochromatic Debye–Scherrer configuration (Section 2.2.4.2), including 1D photodiode arrays (Pennartz *et al.*, 1992; Wong *et al.*, 2006; Palmer *et al.*, 2004), the Mythen curved 1D PSD (Fadenberger *et al.*, 2010), pixel detectors (Yonemura *et al.*, 2006; Terasaki & Komizo, 2011), CCD-based detectors (Malard *et al.*, 2011; Elmer *et al.*, 2007), and medical-imaging detectors (Chupas, Chapman, Jennings *et al.*, 2007; Newton *et al.*, 2010). The former of these last two studies shows that these large detectors working at hard X-ray energies above 60 keV register a wide enough Q range in a single cycle to allow PDF analysis to be made, thus allowing the conduct of time-resolved PDF analysis of, for example, catalytic systems composed of evolving nanoparticles. For the latter study, the diffraction measurements were combined with simultaneous monitoring of the reacting system with the acquisition of complementary mass and diffuse reflectance infrared Fourier transform spectra (DRIFTS).

2.2.5.7.2. *Using the pulse structure*

For investigating very fast, reversible processes, use can be made of the bunch structure of the synchrotron source and the stroboscopic measurement approach. The time for an orbit of an electron circulating in a synchrotron is (circumference/c) s. For a synchrotron such as at the ESRF (with a circumference of 844.4 m), this corresponds to 2.82 µs (*i.e.* a frequency of 355036 Hz). Thus when operating with 16 electron bunches distributed evenly around the ring, there is a burst of X-rays delivered to a beamline every 176 ns, and because of the longitudinal dimension of the electron bunch (∼20 mm), each burst lasts ∼70 ps. Such a pulsed source can be used in pump–probe powder-diffraction experiments, whereby a sample is excited by a short laser pulse (∼100 fs duration) then probed by the X-ray beam a chosen delay time later. The scattered X-rays are recorded with a suitable (probably 2D) detector and the process is repeated, with the statistical quality of the diffraction pattern building up over a number of cycles, after which the detector is read out. A high-speed chopper in the X-ray beam can be used to select the pulse frequency desired for any particular set of measurements. By varying the delay time the evolution of the sample as a function of time after the initial excitation can be investigated. The whole experiment needs fast, accurate electronics to correlate the timing of the firing of the laser, the arrival of the X-ray pulse and the phasing of the chopper.

Examples include the study of 4-(dimethylamino)benzonitrile and 4-(diisopropylamino)benzonitrile (Davaasambuu *et al.*, 2004; Techert & Zachariasse, 2004), whose fluorescence properties indicate that photoexcitation leads to the formation of an intramolecular charge-transfer state. Powder-diffraction patterns were collected over 10-minute periods at a frequency of 897 Hz at delay times ranging from −150 ps (as a reference before the laser excitation) to +2500 ps after excitation. Only about 5% of the molecules are excited by the laser, so the powder-diffraction pattern is from a sample containing both excited and ground-state molecules. Rietveld refinement of the structures from the diffraction patterns gave the fraction of excited molecules as a function of delay time, and the nature of the structural change induced by the photoexcitation. For the isopropyl analogue, an exponential relaxation time of 6.3 (±2.8) ns was observed for the excited molecules (compared to 3.28 ns seen spectroscopically). The main distortion to the molecules was a change in the torsion angle between the diisopropylamino group and the benzene ring, from 13–14° determined from the pre-excitation patterns (14.3° *via* single-crystal analysis) to 10 (±1–2)°.

2.2.5.8. *Beamline evolution*

A beamline at a synchrotron source will certainly evolve in its specifications and capabilities. Users and prospective users should follow updates on a facility's website, or contact the beamline staff, for information concerning possibilities for experiments.

References

Als-Nielsen, J. & McMorrow, D. (2001). *Elements of Modern X-ray Physics*. New York: Wiley.

Authier, A. (2006). *Dynamical theory of X-ray diffraction. International Tables for Crystallography*, Vol. B, *Reciprocal Space*, 1st online ed., ch. 5.1. Chester: International Union of Crystallography.

Azároff, L. V. (1955). *Polarization correction for crystal-monochromatized X-radiation*. *Acta Cryst.* **8**, 701–704.

Balzar, D. & Ledbetter, H. (1993). *Voigt-function modeling in Fourier analysis of size- and strain-broadened X-ray diffraction peaks*. *J. Appl. Cryst.* **26**, 97–103.

Barnes, P., Jupe, A. C., Colston, S. L., Jacques, S. D., Grant, A., Rathbone, T., Miller, M., Clark, S. M. & Cernik, R. J. (1998). *A new three-angle energy-dispersive diffractometer*. *Nucl. Instrum. Methods Phys. Res. B*, **134**, 310–313.

Beaumont, J. H. & Hart, M. (1974). *Multiple Bragg reflection monochromators for synchrotron X radiation*. *J. Phys. E Sci. Instrum.* **7**, 823–829.

Bergamaschi, A., Cervellino, A., Dinapoli, R., Gozzo, F., Henrich, B., Johnson, I., Kraft, P., Mozzanica, A., Schmitt, B. & Shi, X. (2009). *Photon counting microstrip detector for time resolved powder diffraction experiments*. *Nucl. Instrum. Methods Phys. Res. A*, **604**, 136–139.

Bergamaschi, A., Cervellino, A., Dinapoli, R., Gozzo, F., Henrich, B., Johnson, I., Kraft, P., Mozzanica, A., Schmitt, B. & Shi, X. (2010). *The MYTHEN detector for X-ray powder diffraction experiments at the Swiss Light Source*. *J. Synchrotron Rad.* **17**, 653–668.

Bilderback, D. H. (1986). *The potential of cryogenic silicon and germanium X-ray monochromators for use with large synchrotron heat loads*. *Nucl. Instrum. Methods Phys. Res. A*, **246**, 434–436.

Boccaleri, E., Carniato, F., Croce, G., Viterbo, D., van Beek, W., Emerich, H. & Milanesio, M. (2007). *In situ simultaneous Raman/high-resolution X-ray powder diffraction study of transformations occurring in materials at non-ambient conditions*. *J. Appl. Cryst.* **40**, 684–693.